HHS Public Access

Author manuscript

Neuroimage. Author manuscript; available in PMC 2018 March 07.

Published in final edited form as:

Neuroimage. 2017 February 01; 146: 821–832. doi:10.1016/j.neuroimage.2016.09.037.

Convergence of prefrontal and parietal anatomical projections in a connectional hub in the striatum

Eun Young Choi, **Yoko Tanimura**, **Priti R. Vage**, **Ellen H. Yates**, and **Suzanne N. Haber***

Department of Pharmacology and Physiology, School of Medicine and Dentistry, University of Rochester Medical Center, Rochester, NY 14642, United States

Abstract

Visual attentional bias forms for rewarding and punishing stimuli in the environment. While this attentional bias is adaptive in healthy situations, it is maladaptive in disorders such as drug addiction or PTSD. In both these disorders, the ability to exert control over this attentional bias is associated with drug abstinence rates or reduced PTSD symptoms, indicating the interaction of visual attention, cognitive control, and stimulus association. The inferior parietal lobule (IPL) is central to attention, while the prefrontal cortex (PFC) is critical for reward, cognitive control, and attention. Importantly, regions of the IPL and PFC commonly project to the rostral dorsal caudate (rdCaud) of the striatum. We propose an anatomical network architecture in which IPL projections converge with PFC projections in a connectional hub in the rdCaud, providing an anatomical substrate for the interaction of these projections and their competitive influence on striatal processing. To investigate this, we mapped the dense projections from the caudal IPL and prefrontal (dlPFC, vlPFC, OFC, dACC, and dmPFC) regions that project to the medial rdCaud with anatomical tract-tracing tracer injections in monkeys. These inputs converge in a precise site in the medial rdCaud, rostral to the anterior commissure. Small retrograde tracer injections confirmed these inputs to the medial rdCaud and showed that a proximal ventral striatal location has a very different pattern of cortical inputs. We next used human resting-state functional connectivity MRI (fcMRI) to examine whether a striatal hub exists in the human medial rdCaud. Seed regions in the human medial rdCaud revealed cortical correlation maps similar to the monkey retrograde injection results. A subsequent analysis of these correlated cortical regions showed that their peak correlation within the striatum is in the medial rdCaud, indicating that this is a connectional hub. In contrast, this peak striatal correlation was not found in the ventral striatal location, suggesting that this site is not a connectional hub of cortical regions. Taken together, this work uses the precision of monkey anatomy to identify a connectional hub of IPL and PFC projections in the medial rdCaud. It also translates this anatomical precision to humans, demonstrating that, guided by anatomy, connectional hubs can be identified in humans with fcMRI. These connectional hubs provide more specific treatment targets for drug addiction, PTSD, and other neurological and psychiatric disorders involving the striatum.

*Correspondence to: Department of Pharmacology and Physiology, University of Rochester School of Medicine and Dentistry, 601 Elmwood Ave. Box 711, Rochester, NY 14642, United States. suzanne_haber@urmc.rochester.edu (S.N. Haber).

Keywords

Striatum; Prefrontal; Parietal; Corticostriatal connectivity; Monkey anatomy; Resting-state functional connectivity

1. Introduction

Visual attentional bias develops during incentive-based learning in response to positively or negatively reinforced stimuli (Anderson et al., 2011a, 2011b; Hickey et al., 2010; Koster et al., 2005; Schmidt et al., 2015). This attentional bias is adaptive in healthy situations; it allows us to quickly procure rewards or avoid punishments in the environment. However, attentional bias can also be maladaptive and strengthen stimulus-outcome associations, leading to the formation of harmful habits such as drug addiction (Field and Cox, 2008; Franken, 2003; Robinson and Berridge, 1993) or nonproductive responses as in post-traumatic stress disorder (PTSD) (Block and Liberzon, 2016; Hayes et al., 2012). In these situations, cognitive control is limited in its ability to mediate between attentional bias and action. Indeed, addiction studies have shown that the degree to which control can be exerted over attentional drug bias correlates with improved abstinence rates (Fadardi and Cox, 2009; Ziaee et al., 2016). Similarly in PTSD, training in keeping one's attention away from threatening stimuli leads to reduced PTSD symptoms (Badura-Brack et al., 2015; Kuckertz et al., 2014; Schoorl et al., 2013). Together, these observations indicate an interaction of visual attention, cognitive control, and stimulus-outcome associations leading to habit development.

The striatum has a well-established, central role in the development of stimuli salience, reinforcement conditioning, and the habitualization of behavior (Everitt et al., 2008; Everitt and Robbins, 2005; Robinson and Berridge, 2001; Yin and Knowlton, 2006). Prior anatomical tract-tracing and human neuroimaging studies have shown that cortical regions processing visual attention, stimulus association, and cognitive control connect with the dorsal caudate of the striatum. Monkey tract-tracing cases show that the orbitofrontal cortex (OFC), ventrolateral prefrontal cortex (vlPFC), dorsolateral prefrontal cortex (dlPFC), dorsomedial prefrontal cortex (dmPFC), and dorsal anterior cingulate cortex (dACC) all project to the dorsal caudate. Interestingly, the inferior parietal lobule (IPL), which is central to visual attention, also projects to the dorsal caudate (Cavada and Goldman-Rakic, 1991; Yeterian and Pandya, 1993). The IPL is involved specifically in attention spontaneously drawn towards behaviorally relevant stimuli (bottom-up or ventral attention) (Corbetta et al., 2008; Corbetta and Shulman, 2002; Steinmetz and Constantinidis, 1995), such as drugs of abuse. Indeed, the IPL, as well as parts of the PFC, shows increased activity during the presentation of drug-related visual stimuli in addiction (e.g., drug paraphernalia) (Garavan et al., 2000; Grant et al., 1996; Kilts et al., 2014; Kühn and Gallinat, 2011; Maas et al., 1998) or viewing emotional stimuli in PTSD (Mazza et al., 2013; Mueller-Pfeiffer et al., 2013).

Human resting-state functional connectivity MRI (fcMRI) and diffusion MRI (dMRI) have indicated the convergence of parietal and PFC connections in the human dorsal caudate. fcMRI has revealed that there is a longitudinal zone involving the rdCaud that is functionally

linked with distributed caudal IPL and prefrontal regions in the dlPFC, vlPFC, and dACC (Barnes et al., 2010; Choi et al., 2012; Di Martino et al., 2008). Importantly, Jarbo and Verstynen (2015) linked these fcMRI findings to dMRI structural connectivity. This study clearly demonstrated that structural connections of the parietal, OFC, and dlPFC converge in a longitudinal zone encompassing the rdCaud. Together, neuroimaging studies reveal an overlap of parietal and PFC connections in the dorsal caudate. However, the specific prefrontal and parietal areas that converge in the dorsal caudate, nor the precise extent and location of this convergence, are not well defined.

Here, using the precision of monkey anatomical tract-tracing, we build upon the prior monkey and human studies by examining whether there is anatomic convergence within the dorsal caudate of the terminal fields of projections from the caudal IPL and the vlPFC, dlPFC, dmPFC, dACC, and OFC, regions involved in visual attention, stimulus-outcome association, and cognitive control (Bush et al., 2000; Fuster, 2008; Levy and Wagner, 2011; Rolls, 2002; Venkatraman and Huettel, 2012). In particular, based on our prior demonstration of a connectional hub of prefrontal projections in the medial caudate (Averbeck et al., 2014), we hypothesized that caudal IPL projections converge with vlPFC, dlPFC, dmPFC, dACC, and OFC projections in a specific connectional hub within the rostral dorsal caudate (rdCaud). This connectional hub would be a unique region within the longitudinal zone identified from fcMRI and dMRI studies that receives the greatest convergence of inputs from multiple regions of parietal cortex, OFC, and dlPFC, as well as of vlPFC, dmPFC, and dACC, which are important for switching behaviors and context-dependent action selection (Bunge, 2004; Rushworth et al., 2002; Toni et al., 1999; Woodward et al., 2006).

To investigate this, we first identified the precise site of convergence in the rdCaud by charting the projections from caudal IPL with those from the vlPFC, dlPFC, dmPFC, dACC, and OFC. To confirm this convergence, we placed retrograde tracer injections in the area of convergence in the medial rdCaud and, using unbiased stereology, identified and quantified the inputs from the caudal IPL and PFC. We also charted the cortical inputs to a proximal ventral caudate location (vCaud) with retrograde tracer injections, which resulted in a very different pattern of cortical inputs. We next used fcMRI in healthy human subjects to examine whether a similar striatal hub architecture of convergent PFC and IPL connections exists in the human rdCaud. The results show that a site in the human medial rdCaud contains converging inputs from the caudal IPL, vlPFC, dlPFC, dmPFC, dACC, and OFC. In contrast, a different set of cortical areas input to the human vCaud. These results provide anatomical evidence for the convergence and interaction of caudal IPL and five prefrontal areas within a connectional hub in the medial rdCaud. Moreover, there is a homologous region or hub within the human caudate with a similar set of convergent inputs. As such, this striatal hub is likely to be central for the influence of visual attention and control on striatal processing.

2. Materials and methods

2.1. Overview

The present study consists of three levels of analyses. First, we identified the location of convergence of caudal IPL and PFC projections in the striatum of monkeys. We placed anterograde tracer injections in input regions to the rdCaud in the caudal IPL, vlPFC, dlPFC, dmPFC, dACC, and caudal OFC, and traced dense terminal projections in the striatum. To compare the labeled anatomy between cases from different monkeys, each case was merged onto a standard monkey brain model. Convergence of projections was assessed and quantified with a heatmap of overlapping projections from each case.

Having identified the medial rdCaud as a connectional hub of the caudal IPL and the above PFC projections, we confirmed and characterized this convergence using small retrograde tracer injections in the medial rdCaud. The pattern of labeled cells in 2 rdCaud cases was compared to those from 2 cases with injections in a proximal ventral caudate location, the vCaud. One case each of the rdCaud and vCaud cases was charted and the density of labeled cells in each cortical area was quantified to determine the strengths of those inputs.

Finally, we examined human fcMRI for evidence of a similar connectional hub in the human rdCaud. The position of the center of the convergence in the monkey rdCaud was determined, and the corresponding human location was identified with the proportionally same spatial location in the human striatum. Using a single 2 mm^3 voxel seed region at this human rdCaud site, a whole brain fcMRI map (N=500) was generated to identify functionally connected cortical regions to the rdCaud and then compared with the monkey anatomy. To confirm that the human medial rdCaud is the major striatal hub of connectivity with these cortical regions, a striatal fcMRI map was created using a seed region of cortical regions with correlations of 1.5 standard deviations or greater above the mean with the medial rdCaud seed region. These results were compared with those of the vCaud, which were obtained with the same process using a single 2 mm^3 voxel seed region at the human vCaud location corresponding to the monkey vCaud injection site.

2.2. Injection sites

6 anterograde cortical injections were placed in prefrontal and parietal regions previously shown to project to the dorsal caudate (Haber et al., 2006; Künzle, 1978; Selemon and Goldman-Rakic, 1985; Yeterian and Van Hoesen, 1978). These were 5 functionally diverse regions of the dlPFC in the dorsal bank of the principal sulcus (area 46), dmPFC (area 9), vlPFC in the ventral limb of the arcuate sulcus (area 45), dACC (area 24), and OFC in the lateral bank of the medial orbital sulcus (area 13). The caudal IPL injection was in the ventral lip of the caudal intraparietal sulcus (areas 7a/PG and 7a/Opt). 4 retrograde striatal injections were placed in the medial rdCaud or vCaud. All injection cases had labeling throughout the cortex and no contamination (tracer leakage into an adjacent cortical area, structure, or white matter).

2.3. Surgery and tissue preparation

10 adult macaque monkeys (3 *Macaca nemestrina*, 4 *Macaca fascicularis*, and 3 *Macaca mulatta*) were used for these tracing studies. All experiments and animal care were conducted in accordance with the *Guide for the Care and Use of Laboratory Animals* (Institute of Laboratory Animal Resources, 1996) and were approved by the University of Rochester's University Committee on Animal Resources. For a subset of experiments, a presurgical T1 (0.5 mm×0.5 mm×0.5 mm) or T2 turbo spin echo MRI scan (0.5 mm×0.5 mm×1.42 mm) was acquired on a 3T Siemens Tim Trio scanner (Siemans, Erlangen, Germany) to aid with stereotactic tracer placement during surgery. For the remaining experiments, serial electrode penetrations were made to locate the anterior commissure and calculate the stereotactic position of target injection sites, as described previously (Haber et al., 1993). Surgical procedures were conducted as previously described (Heilbronner, 2014). Tracers were Lucifer Yellow (LY), Fluororuby (FR), or Fluorescein (FS) conjugated to dextran amine (Invitrogen), wheat germ agglutinin conjugated with horseradish peroxidase (WGA) (Sigma-Aldrich), or tritiated amino acids (AA) (100 nl, 1:1 solution of [^{3}H]-leucine and [^{3}H]-proline in dH_2O, 200 mCi/ml; NEN). 12–14 days post-surgery, animals were deeply anaesthetized with pentobarbital and perfused with saline followed by a 4% paraformaldehyde/1.5% sucrose solution. Brains were postfixed overnight and cryoprotected in increasing gradients of sucrose. Immunocytochemistry was performed on one in eight free-floating 50 μm sections to visualize LY, FR, FS, or WGA tracers, as previously described (Heilbronner, 2014). For autoradiography, one in eight sections were mounted on chrome-alum gel-coated slides and defatted in xylene overnight. Slides were dipped in Kodak NTB2 photographic emulsion and exposed for 4–6 months at 4 °C in a light-tight box. Sections were developed in Kodak D19, fixed, washed, and counterstained with cresyl violet.

2.4. Anterograde cortical projection analysis

For the prefrontal and parietal anterograde injection cases, dark field light microscopy under 1.6×, 4×, and 10× objectives was used with Neurolucida software (MicroBrightField) to trace outlines of dense, focal projection patches in the striatum in one in eight sections from the rostral end of the striatum to at least the level of the anterior commissure. Dense projections were defined as terminal fields visible at 1.6× with discernible boundaries. Tracings of striatal focal projections from each case were merged onto a 3-D global reference brain model developed from one animal, as described previously (Haber et al., 2006) in the following manner. 2-D tracings of each section created in Neurolucida were imported as a stack into IMOD, a 3-D rendering program (Boulder Laboratory for 3D Electron Microscopy of Cells, University of Colorado, Boulder, CO) (Kremer et al., 1996). Merging of each case to the standard brain was done with a linear transformation in IMOD using anatomical landmarks (e.g., gyri, sulci, white and gray matter structures) and then checked and adjusted by hand. Cases were rendered in 3-D and checked with the tracings in the original brain to have the same anterior-posterior, dorsal-ventral, and medial-lateral placement and relative size. Each case was merged onto the global reference brain independently of one another. To quantify the overlap of prefrontal and parietal focal projections in the striatum, we created a heatmap of the overlap as follows. For each case, the 3-D rendered dense projections were used to obtain dense projection contours on

consecutive sections of the standard monkey striatum using the IMOD functions *imodfillin* and *imodmop*. These dense projection patterns were spatially summed to create a heatmap in which the values of the map indicate the number of cases contributing to the overlapping projections. This heatmap allowed us to identify the site of greatest convergence in the striatum.

2.5. Retrograde striatal injection analysis

For striatal injection cases, dark and light field light microscopy under 20X objective was used to identify retrogradely labeled input cells. For 1 case each of the rdCaud and vCaud injections, labeled cells were counted throughout the cerebral cortex in one in twenty-four sections. StereoInvestigator software (MicroBrightField) was used to stereologically count labeled cells with an even sampling (64%) and then multiplied by 1.5625 to estimate the total number of cells. The total cell number was divided by the total area sampled to obtain the density of input cells in each brain area. To estimate cytoarchitectonic areal boundaries, we used the atlas by Paxinos et al. (2000) in conjunction with detailed anatomical descriptions (Pandya and Seltzer, 1982; Preuss and Goldman-Rakic, 1991; Vogt, 1993; Vogt, 2009). Identified areas of input were confirmed in the second rdCaud and vCaud injection cases. 3-D IMOD models were created with the same procedure as described above for Neurolucida tracings. The statistical difference in the rdCaud and vCaud inputs for the 13 cortical areas in Fig. 5 was assessed using a chi-square test to determine the goodness-of-fit of the distribution of cell densities for the vCaud versus that for the rdCaud. Due to the different total sums of cell densities in the rdCaud and vCaud cases, the test was performed on the percent cell densities for each case.

2.6. Resting-state functional connectivity MRI analysis

All fcMRI analyses were conducted on 500 healthy adult subjects (mean age =21.3 yr, 18–35 yr; 42.6% male; 91% right handed) from a publicly available, fully preprocessed dataset (Brain Genomics Superstruct Project, http://neuroinformatics.harvard.edu/gsp). This cohort of subjects was examined as the Discovery sample in prior studies (Choi et al., 2012; Yeo et al., 2011). To test whether the findings reported here could be seen in smaller groups, subsets of n=10, 20, 30, 40, 50, 100, or 150 were created from this dataset of 500 subjects. These groups were matched for mean age, gender, race, ethnicity, and handedness to the larger dataset of N=500.

Briefly, data were acquired on a 3T Siemens Tim Trio MRI scanner (3 mm×3 mm×3 mm). One or two resting-state (eyes open, no fixation) runs were obtained per subject (each 6 min 12 s, mean=1.7 runs). Data were preprocessed using SPM2 (Wellcome Department of Cognitive Neurology, London, UK) and FSL (Jenkinson et al., 2012; Smith et al., 2004) and included slice time correction, atlas normalization, motion correction, global mean regression, regression of ventricle and white matter signal, and low-pass filtering at 0.08 Hz. Structural and functional data were processed into the fsaverage5 volume (2 mm isotropic resolution) and cortical surface using FreeSurfer 4.5.0 (http://surfer.nmr.mgh.harvard.edu) and Gaussian smoothing was applied (6 mm FWHM kernel). Data that did not undergo Gaussian smoothing were used for the nonsmoothed data analysis. See Choi et al. (2012), Holmes et al. (2015) and Yeo et al. (2011) for further details. An additional striatal

regression was performed of the signal from cortical voxels within 4.5 mm of the putamen to remove signal contamination between the striatum and adjacent cortex, as previously described (Choi et al., 2012).

fcMRI analyses were conducted as previously described (Choi et al., 2012). For each subject, Pearson's product-moment correlations were computed between the FreeSurfer fsaverage5 striatal volume and cortical surface. These individual *r* maps were converted to *z* maps with Fisher's *r*-to-*z* transformation and combined to create group mean *z* maps, correcting for multiple comparisons with the Bonferroni correction. Cortical correlations were projected onto the Caret surface for display purposes. Due to the very large number of subjects in the dataset (N=500), even the weakest correlations were highly significant (1 sample *t*-test) and passed a Bonferroni correction. Thus, statistically based thresholding of fcMRI maps was not useful here. Instead, we examined the strongest correlations in each map at a threshold (greater than 1.5 standard deviations above the mean correlation) that highlighted the topographical differences between the rdCaud and vCaud maps. The threshold of group mean fcMRI maps displayed in Caret was set at r(z)=0.1 or r(z)=0.07 for the smoothed and nonsmoothed data, respectively, a cut-off value that corresponded approximately to 1.5 standard deviations of the mean for both rdCaud and vCaud maps.

Seed regions were selected as follows. The center of the greatest overlap of prefrontal and parietal projections was identified in the monkey rdCaud from the heatmap of anterograde projections. The convergence site's relative anterior-posterior, dorsal-ventral, and medial-lateral position was determined between the rostral end of the caudate and the start of the anterior commissure and within a rectangular area parallel to the midline and boxing the caudate and adjacent nucleus accumbens on that section (Fig. 6). The spatially proportionate human rdCaud location (−10, 10, 14) was identified within a proportionally sized box placed in the same way in a 1 mm^3 FSL MNI152 template in Montreal Neurological Institute (MNI) space (available for download https://surfer.nmr.mgh.harvard.edu/fswiki/StriatumParcellation_Choi2012). Similarly, the relative position of the center of the vCaud injection was used to find the spatially proportionate human vCaud location (−9, 9, 5). Single voxel 2 mm^3 striatal seed regions were created centered on the corresponding FreeSurfer coordinates. Cortical seed regions were obtained by creating masks of all cortical surface vertices with group mean z(r) correlations greater than 1.5 standard deviations above the mean correlation within these striatal seed region-derived fcMRI maps.

3. Results

3.1. Striatal projections from the prefrontal cortex

We examined dense corticostriatal projection patterns from prefrontal regions involved in visual attention, reward, and cognitive control (Fig. 1). Surrounding diffuse projections were present, providing broad light innervation, but were not included in the analysis due to inaccuracies in outlining their relatively indistinct borders. In general, dense projections from the dlPFC, dmPFC, and vlPFC project primarily to the dorsal caudate with smaller patches in the putamen. Within this pattern, projections from the dlPFC and dmPFC to the putamen primarily terminate medially, while those from vlPFC terminate both medially and laterally in the putamen. Inputs from the dACC and OFC generally terminate in a broad

territory covering both the dorsal and ventral caudate and putamen, with OFC projections terminating more ventrally into the nucleus accumbens. Despite the variations in these projection patterns, as well as the functional diversity of their cortical origins, all of these projections target the rdCaud and, to a lesser extent, the medial putamen. As such, the rdCaud was the prime candidate for a site of integration across visual attention, reward, and cognitive control.

3.2. Striatal projections from the caudal IPL

To pinpoint where in the rdCaud the projections from caudal IPL converged with prefrontal projections described above, we charted the projections from the caudal IPL to the striatum. An injection in the caudal IPL (area 7a/PG) resulted in projections terminating in the dorsal caudate, particularly along the dorsal edge of the caudate and extending ventrally (Fig. 2). These projections terminated longitudinally in the head and body of the caudate until the level of the anterior commissure. Like prefrontal projections, caudal IPL projections terminated in dense patches with a broader, surrounding area of diffuse innervation. In addition to these projections to the dorsal caudate, small dense patches were seen in the tail of the caudate (not shown). The putamen contained few dense projection patches, which were located along the dorsomedial edge of the rostral putamen and in the mid and ventral caudal putamen (not shown). This topography of projections is similar to those from a prior study using a tritiated amino acid anterograde tracer injection in approximately the same location in the caudal IPL (Fig. 2) (Selemon and Goldman-Rakic, 1985). Consistent with its larger injection size, this previously reported case showed wider spread but topographically similar label in the rdCaud, including along the dorsal edge, and the body of the caudate.

3.3. Convergence of caudal IPL and prefrontal projections in the rostral dorsal caudate

Dense projections from the prefrontal and caudal parietal cases were merged onto a standard brain to examine overlap between cases. Overall, caudal IPL projections were located more dorsolaterally in the rdCaud, primarily along its dorsal borders (Fig. 3B). Overlap occurred between prefrontal and the ventral-most IPL projections in the rdCaud. A heatmap quantifying the overlap of these prefrontal and parietal cases showed that these projections form a longitudinal zone of convergence throughout the rostro-caudal extent of the caudate. Within this longitudinal convergence zone, the greatest overlap was located medially in the rdCaud, approximately 2 mm rostral to the anterior commissure (Fig. 3C). Here, the ventral-most caudal IPL projections directly converged with those from the dlPFC, vlPFC, dmPFC, and the caudal OFC (Fig. 3B) and were proximal to those from the dACC. Taken together, these results show that caudal IPL projections converge in the medial rdCaud with those from visual attention, cognitive control, and reward-related PFC regions.

3.4. Retrogradely labeled cortical inputs to the rostral dorsal caudate and ventral caudate

In order to verify the convergence of prefrontal and parietal inputs to the medial rdCaud, a small retrograde tracer injection was placed at approximately the site of the convergence area in the medial rdCaud. Retrogradely labeled cortical input cells were charted (Fig. 4A; Fig. 7A) and quantified (Fig. 5). The injection resulted in labeled cells in the dlPFC, dmPFC, vlPFC, dACC, OFC, and the caudal IPL. The primary input was from area 9/46d, as well as additional inputs from areas 9 and 8. Inputs also came from other dlPFC regions in

areas 46 and 10, as well as from area 44/45 in the vlPFC and area 24 in the dACC. While not as numerous as for the PFC, the parietal cortex also sent dense inputs from a small, localized part of the caudal IPL in area Opt that continued into the caudal end of area PG. Few inputs were seen from ventral PFC regions, including areas 9/46v, 47, 11/13 in the OFC, and 14, 25, and 32 in the mPFC and vmPFC. Although not the focus of this study, labeled cells were also seen in posteromedial and temporal regions. These cases confirmed that dlPFC, dmPFC, vlPFC, dACC, OFC, and caudal IPL projections converge in a restricted location of the medial rdCaud.

As a comparison to the rdCaud inputs, we examined the labeled cortical inputs from a small retrograde tracer injection in a proximal ventral location in the vCaud. Retrogradely labeled cortical input cells were charted (Fig. 4B; Fig. 7C) and quantified (Fig. 5). Overall, there were fewer labeled cells across the cortex than in the rdCaud cases, which is likely due to differences in tracer uptake and transport. Nonetheless, these vCaud cases showed a different set of cortical inputs to the vCaud primarily from ventral PFC regions and none from the IPL ($X^2(12,100)=1560$, $p < 0.0001$). These inputs were primarily from area 47 in the vlPFC, area 11/13 in the OFC, and area 9/46v in the ventral lip of the principle sulcus. Labeled cells were also seen in area 44/45 in the vlPFC, areas 25 and 14 in the vmPFC, area 9 in the rostral dlPFC, and area 24 in the dACC. Lighter label was seen in areas 10, 8, 9/46d, and 46 of the dlPFC. No labeled cells were seen in the caudal IPL. Labeled cells were also observed in posteromedial and temporal regions. Overall, the rdCaud and vCaud receive considerably different patterns of cortical inputs, indicating the specificity of the information integrated in each striatal region.

3.5. A connectional hub in the human rostral dorsal caudate

A human fcMRI map was generated from 500 healthy human subjects using a single 2 mm^3 voxel seed region in the rdCaud and underwent a Bonferroni correction for multiple comparisons. The seed region was placed at the spatially proportionate location in the human rdCaud (−10, 10, 14) as the center of the greatest convergence of IPL and PFC projections in the monkey rdCaud (Fig. 6A). Seed region placement in neighboring voxels of the medial rdCaud yielded qualitatively similar cortical fcMRI maps. Overall, the broad pattern of the strongest correlations was consistent with the monkey anatomical connections (Fig. 7A). The strongest correlations with the human rdCaud were seen with parts of the IPL, dlPFC, vlPFC, dACC, and dmPFC (Fig. 7B; negative correlations in Supplementary Fig. 1A). Weaker correlations below the threshold were seen in the vmPFC and OFC, consistent with the weak or absent projections from the monkey vmPFC and OFC to the monkey rdCaud. In contrast, the human vCaud had a distinctly different fcMRI correlation map from the human rdCaud map (Fig. 7D; negative correlations in Supplementary Fig. 1B) that resembled the pattern of cortical projections to the monkey vCaud (Fig. 7C). This fcMRI map was generated with a single 2 mm^3 voxel seed region placed in the human vCaud at the spatially proportionate location (−9, 9, 5) as the center of the monkey vCaud injection site (Fig. 6B) and underwent a Bonferroni correction for multiple comparisons. Seed region placement in neighboring voxels of the vCaud yielded qualitatively similar cortical fcMRI maps. As with the monkey anatomy, the strongest correlations with the human vCaud were seen with ventral PFC regions, specifically the inferior frontal and

rostral middle frontal gyri, as well as the dACC and dmPFC. Unlike the human rdCaud map, weak or no correlations were seen with the IPL and caudal regions of the dlPFC (i.e., caudal superior and middle frontal gyri), consistent with the monkey anatomy.

To confirm that the medial rdCaud is indeed the connectional hub of visual attention, reward, and cognitive control cortical inputs to the human striatum, we computed the striatal fcMRI correlations of the cortical regions identified from the rdCaud map above to identify whether they are indeed most strongly correlated with the medial rdCaud or elsewhere in the striatum. This striatal fcMRI analysis was performed in the same dataset used to derive the rdCaud fcMRI map in order to answer whether the medial rdCaud is the connectional hub for its specific set of cortical input regions. Using a single large seed region composed of all cortical regions with z(r) correlations greater than 1.5 standard deviations above the mean ($z(r) > 0.1308$) with the rdCaud seed region, we found that the medial rdCaud is indeed the site in the human striatum that is most strongly functionally connected to these cortical regions (Fig. 8A; negative correlations in Supplementary Fig. 2A). The peak correlation was located (−11, 10, 15) proximal to the rdCaud seed region. In contrast, the same analysis for the vCaud seed region showed that the strongest correlations did not occur in the vCaud (Fig. 8B; negative correlations in Supplementary Fig. 2B). A striatal fcMRI map generated from cortical regions with z(r) correlations greater than 1.5 standard deviations above the mean ($z(r) > 0.1013$) with the vCaud seed region revealed correlations that were strongest in a more dorso-lateral location in the caudate (−13, 10, 10), indicating that the vCaud is not the connectional hub of interactions for these cortical regions. Together, these results indicate that the human medial rdCaud is the site of a critical striatal hub linked to the human IPL, vlPFC, dlPFC, dmPFC, and dACC.

3.6. Corticostriatal connectivity in nonsmoothed data and smaller subject groups

In order to check whether the smoothing kernel used here (6 mm FWHM) had an effect on the results, we repeated the analyses with the same data, but nonsmoothed. Overall, correlation values were lower, as expected from nonsmoothed data. The results were similar to those of the smoothed data for the rdCaud seed region's correlations to the cortex (Supplementary Fig. 3A) and their correlations to the striatum (cortical seed region threshold set at $z(r)=0.0674$; peak coordinate was unchanged at −11, 10, 15) (Supplementary Fig. 4A). The results differed somewhat for the vCaud from those of the smoothed data. The vCaud seed region was correlated more strongly with a larger extent of the caudal middle frontal gyrus and parietal lobe (negative correlations shown in Supplementary Fig. 3B) and their peak correlation in the striatum was located more caudally (−14, 3, 16) than in the smoothed data (−13, 10, 10) (cortical seed region threshold set at $z(r) =0.0603$) (Supplementary Fig. 4B). Nonetheless, these data are consistent with our conclusion that the rdCaud is a connectional hub, while the vCaud is not.

We also tested whether the findings from N=500 can be seen in smaller groups of n=10, 20, 30, 40, 50, 100, and 150 subjects drawn from the original dataset (N=500). For the rdCaud, results from groups of n=30 and greater replicated those of N=500 (see Supplementary Table 1 for a comparison of striatal coordinates of peak correlation). However, consistent with the greater ventral striatal variability detected above with the nonsmoothed data, results with the

vCaud were similar, but showed some non-specific variability in the cortical fcMRI maps for the groups of n=10 through n=100 compared to N=500. This was also seen in the peak striatal correlations of these groups, which were located with seemingly random variability around the peak correlation coordinate (−13, 10, 10) for N=500 (Supplementary Table 1). Replication of the N=500 results was seen with the n=150 group, which included the same peak correlation coordinate.

4. Discussion

4.1. Convergence of parietal and prefrontal projections in a connectional hub in the medial rostral dorsal caudate

Behavioral observations of attentional bias indicate the interaction of visual attention, stimulus association, and cognitive control. We hypothesized that anatomical projections from parietal and prefrontal regions converge in a connectional hub in the striatum, providing an anatomical substrate that may underlie this functional interaction. Our results show that caudal IPL projections converge with those from prefrontal cortex (dlPFC, vlPFC, OFC, dACC, and dmPFC) most strongly in a precise site within the striatum, forming a connectional hub of interaction. This site is located in the medial half of the rdCaud at an intermediate coronal level in the caudate, rostral to the anterior commissure. The site specifically avoids the area immediately adjacent to the medial wall of the caudate, which is targeted by vmPFC projections. In contrast to the rdCaud, the vCaud receives projections primarily from ventral lateral prefrontal cortex, dACC, and dmPFC, but does not receive parietal projections. This highlights that the medial rdCaud is a unique hub in the caudate in which visual attention, cognitive control, and reward information are integrated and positioned to affect downstream striatal processing. We note that important hubs mediating these functional interactions may also exist in other brain structures we have not examined, including, but not limited to, the thalamus. Guided by the precision of these monkey anatomical results, we used fcMRI to identify this striatal connectional hub in humans. We found that the human medial rdCaud contains a region with the strongest convergent inputs from the IPL, dlPFC, vlPFC, dACC, and dmPFC regions, identifying a likely homologous human connectional hub. In contrast, as seen with the monkey vCaud anatomy, the human vCaud region is most strongly functionally connected to ventral lateral regions such as the rostral middle and inferior frontal gyri, as well as the dACC and dmPFC. Taken together, these results identify a multi-modal connectional hub of caudal IPL and vlPFC, dlPFC, dmPFC, dACC, and caudal OFC projections in the medial rdCaud that provides an anatomical substrate for the interaction of visual attention, stimulus association, and cognitive control.

4.2. Multiple connectional hubs in the striatum

Early anatomical studies, later supported by viral vector studies, placing relatively large injections in broad cortical functional regions demonstrated the topography of connections between the cortex, basal ganglia, and thalamus (Heimer and Wilson, 1975; Kelly and Strick, 2004; for review, see Alexander et al. (1986) and Haber et al. (2012)). This maintenance of a broad functional topography served as the basis for the parallel circuits model in which there are segregated corticobasal ganglia-thalamic loops dedicated to

different functions (Alexander et al., 1986; DeLong and Georgopoulos, 1981). Later studies using small, specific injections in a number of different prefrontal areas discovered that within this broad functional topography, corticostriatal projections highly overlap with one another, indicating a high degree of integration across functional territories (Calzavara et al., 2007; Haber et al., 2006). Importantly, this convergence is not simply overlap at the boundaries of projection terminal fields. Rather, a hub architecture exists such that there are regions within the striatum that receive a high convergence of inputs from diverse functional regions, forming connectional hubs of integration. Previously, we showed an area within the medial caudate that receives a combination of inputs from prefrontal cognitive areas mediating different aspects of reinforcement learning (Averbeck et al., 2014). The present study demonstrates a connectional hub located further dorsally in the medial rdCaud pertinent to the control of attentional bias. This hub involves the interaction of connections from visual attention, stimulus-outcome association, and cognitive control cortical regions. Furthermore, there are likely to be multiple connectional hubs in the striatum associated with different functional interactions. Indeed, Gerbella et al. (2015) showed that projections from hand-related regions in the premotor cortex, vlPFC, and IPL have high convergence in the striatum that may be the possible site of a connectional hub for hand-related functions.

4.3. Implications for human neuroimaging studies of corticostriatal connectivity

Resting-state fcMRI and dMRI studies of human corticostriatal connectivity generally have found results that broadly replicate the motor-association-limbic functional gradient in the striatum (Barnes et al., 2010; Di Martino et al., 2008; Draganski et al., 2008; Leh et al., 2007; Lehéricy et al., 2004; Verstynen et al., 2012). In addition, previous fcMRI studies have demonstrated the functional convergence of distributed parietal and prefrontal connections within the rdCaud (Barnes et al., 2010; Choi et al., 2012; Di Martino et al., 2008). Jarbo and Verstynen (2015) provided the first clear evidence in humans that the underlying structural connections from distributed prefrontal and parietal regions also converge in the rdCaud. However, the inability to do invasive tract-tracing leads to some limitations in investigating the topography in humans. Monkey anatomy, while subject to species differences, complements the knowledge provided by human neuroimaging. The present anatomical results confirm the convergence of prefrontal and parietal connections in the rdCaud, but also more precisely pinpoint the location of the hub. Moreover, it provides key information about the specific cortical areas that constitute the hub. Guided by these anatomical results, our fcMRI analyses showed that the spatially proportionate site in the human medial rdCaud is linked to a similar distributed set of regions in the IPL and the dlPFC, vlPFC, dACC, and dmPFC. This site is the most strongly correlated striatal location with these cortical regions, suggesting that it is the homologous human connectional hub. This human rdCaud hub is consistent with parcellations of the striatum based on corticostriatal fcMRI (Barnes et al., 2010; Choi et al., 2012), suggesting that these parcellations predict the locations of other connectional hubs within the striatum.

4.4. fMRI signal variability in the ventral striatum

Prior studies have shown that smoothing, while improving the signal-to-noise ratio, can produce artifactual shifting of activity (Geissler et al., 2005; Jo et al., 2008; Jo et al., 2007; White et al., 2001). In particular, Sacchet and Knutson (2013) reported that larger smoothing

kernels systematically bias the localization of task-based fMRI activity in the nucleus accumbens in a caudal direction. We found that smoothing did not affect the peak of correlation for the rdCaud-based analysis. As with the smoothed data, the nonsmoothed data showed that the cortical regions derived from the rdCaud seed region are most strongly correlated with the medial rdCaud, suggesting that this is a connectional hub in the striatum. However, consistent with a significant role for smoothing noted by Sacchet and Knutson, we observed that smoothing for the vCaud leads to more spatially specific correlations in the cortex and a primarily rostral shift in the peak striatal correlation of the cortical regions derived from the vCaud (Note: this shift is in the opposite direction of the effect seen by Sacchet and Knutson and may be driven primarily by the lack of smoothing on the selection of the most strongly correlated regions for the cortical seed region, i.e., the inclusion of more caudal cortical regions.). These results do not change the present conclusion that the medial rdCaud is a connectional hub, while the vCaud is not. However, these results and those of Sacchet and Knutson indicate an important consideration of striatal fMRI: the greater signal variability in the ventral striatum (referring to the ventral caudate, ventral putamen, and the nucleus accumbens) in comparison to the dorsal striatum and the impact of smoothing on task-based and resting-state fMRI. The greater signal variability in the ventral striatum was also observable in the analysis with subsets of subjects, which is particularly relevant for clinical studies with limited numbers of subjects. The peak striatal correlation from the rdCaud-derived cortical regions of the larger dataset was replicated with as few as 30 subjects. However, the peak coordinates for the vCaud showed seemingly non-specific variability around the peak coordinate from N=500 subjects, which was replicated only in the group of n=150. This signal variability in the ventral striatum may be due to technical and/or biological reasons. Technically, the ventral striatum is more susceptible than the dorsal striatum to the signal dropout from the nasal cavities, which would result in greater noise-related random variation in the signal. Biologically, the vCaud seed region is located next to the internal capsule, while the rdCaud seed region is located farther away along the medial edge of the caudate. In addition to the main bulk of white matter, the internal capsule has adjacent islands of fibers in different locations across individuals that could increase the variability of the fMRI signal near the boundaries of the internal capsule. In practice, at lower sample sizes, setting higher thresholds may be necessary to replicate the findings from larger datasets. These results underscore the consideration needed when comparing between datasets, particularly for the ventral striatum. A systematic examination of the variability of the fMRI signal in the striatum is needed to clarify this issue.

4.5. Implications of a hub architecture for psychiatric disorders

Addiction involves a complex interplay of various processes involved in forming and controlling the drug habit, including the development of an attentional bias for drugs that promotes drug intake and hinders abstinence (Field and Cox, 2008; Robinson and Berridge, 1993). Similarly in PTSD, excessive trauma leads to an exaggerated, inflexible fear response and attentional bias for associated stimuli (Block and Liberzon, 2016; Hayes et al., 2012). The present results show that the cortical regions underlying these various processes send projections that converge in a connectional hub of the rdCaud. This connectional hub provides a single site within the striatum in which these cortical regions can interact and directly modulate striatal processing. More broadly, identifying connectional hubs is key for

probing both normal behaviors and neurological and psychiatric disorders. These may particularly include disorders that, like addiction and PTSD, involve sensory cues that trigger an automated response. This may include, for example, obsessive-compulsive disorder (OCD) in which environmental cues can trigger highly repetitive rituals in patients, such as repeated hand washing to remove contamination (American Psychiatric Association, 2013; Graybiel and Rauch, 2000). There may be abnormally functioning striatal hubs specific to different disorders. Here, we have demonstrated that a human region with similar connectivity as the rdCaud hub in monkey can be identified using non-invasive fcMRI. Guided by anatomy and identified with neuroimaging, this hub architecture of corticostriatal projections provides new, more specific treatment targets for striatum-related disorders.

4.6. Conclusions

We have used the precision of anatomy to identify the precise prefrontal and parietal cortical regions that converge in the medial rdCaud to form a connectional hub. These cortical areas underlie visual attention, stimulus association, and cognitive control, suggesting a striatal location that may be central to mediating control of attention. We note that there may be hubs in other brain structures we have not examined that also play a role in this interaction. Importantly, the human medial rdCaud contains a similar connectional hub in the medial rdCaud. Together, these results link the precision of an animal tracing study with fcMRI to demonstrate, that in addition to a broad functional gradient, cortical projections have a hub architecture. These connectional hubs provide more specific targets for functional investigation and for probing abnormalities in addiction, PTSD, OCD, and other neurological and psychiatric disorders involving the striatum.

Supplementary Material

Refer to Web version on PubMed Central for supplementary material.

Acknowledgments

This work was funded by National Institute of Mental Health Grants MH 045573 and MH 106435. We thank Drs. Rita Goldstein, Hesheng Liu, Randy Buckner, and Sarah Heilbronner for valuable discussion and Dr. Julia Lehman, Anna Borkowska-Belanger, and Dr. Wei Tang for expert technical assistance. Data were provided [in part] by the Brain Genomics Superstruct Project of Harvard University and the Massachusetts General Hospital (Principal Investigators: Randy Buckner, Joshua Roffman, and Jordan Smoller) with support from the Center for Brain Science Neuroinformatics Research Group, the Athinoula A. Martinos Center for Biomedical Imaging, and the Center for Human Genetic Research. 20 individual investigators at Harvard and MGH generously contributed data to GSP Open Access Data Use Terms Version: 2014-Apr-22 the overall project. The authors declare no competing financial interests.

Appendix A. Supplementary material

Supplementary data associated with this article can be found in the online version at http://dx.doi.org/10.1016/j.neuroimage.2016.09.037.

Abbreviations

rdCaud	rostral dorsal caudate
vCaud	ventral caudate

fcMRI resting-state functional connectivity MRI

References

Alexander GE, DeLong MR, Strick PL. Parallel organization of functionally segregated circuits linking basal ganglia and cortex. Annu Rev Neurosci. 1986; 9:357–381. [PubMed: 3085570]

Anderson BA, Laurent PA, Yantis S. Learned value magnifies salience-based attentional capture. PLoS One. 2011a; 6:e27926. [PubMed: 22132170]

Anderson BA, Laurent PA, Yantis S. Value-driven attentional capture. Proc Natl Acad Sci USA. 2011b; 108:10367–10371. [PubMed: 21646524]

American Psychiatric Association. Diagnostic and Statistical Manual of Mental Disorders. American Psychiatric Publishing; Arlington, VA: 2013.

Averbeck BB, Lehman J, Jacobson M, Haber SN. Estimates of projection overlap and zones of convergence within frontal-striatal circuits. J Neurosci. 2014; 34:9497–9505. [PubMed: 25031393]

Badura-Brack AS, Naim R, Ryan TJ, Levy O, Abend R, Khanna MM, McDermott TJ, Pine DS, Bar-Haim Y. Effect of attention training on attention bias variability and PTSD symptoms: randomized controlled trials in Israeli and U.S. combat veterans. Am J Psychiatry. 2015; 172:1233–1241. [PubMed: 26206075]

Barnes KA, Cohen AL, Power JD, Nelson SM, Dosenbach YB, Miezin FM, Petersen SE, Schlaggar BL. Identifying basal ganglia divisions in individuals using resting-state functional connectivity MRI. Front Syst Neurosci. 2010; 4:18. [PubMed: 20589235]

Block SR, Liberzon I. Attentional processes in posttraumatic stress disorder and the associated changes in neural functioning. Exp Neurol. 2016

Bunge SA. How we use rules to select actions: a review of evidence from cognitive neuroscience. Cogn Affect Behav Neurosci. 2004; 4:564–579. [PubMed: 15849898]

Bush G, Luu P, Posner MI. Cognitive and emotional influences in anterior cingulate cortex. Trends Cogn Sci. 2000; 4:215–222. [PubMed: 10827444]

Calzavara R, Mailly P, Haber SN. Relationship between the corticostriatal terminals from areas 9 and 46, and those from area 8A, dorsal and rostral premotor cortex and area 24c: an anatomical substrate for cognition to action. Eur J Neurosci. 2007; 26:2005–2024. [PubMed: 17892479]

Cavada C, Goldman-Rakic PS. Topographic segregation of corticostriatal projections from posterior parietal subdivisions in the macaque monkey. Neuroscience. 1991; 42:683–696. [PubMed: 1720224]

Choi EY, Yeo BT, Buckner RL. The organization of the human striatum estimated by intrinsic functional connectivity. J Neurophysiol. 2012; 108:2242–2263. [PubMed: 22832566]

Corbetta M, Patel G, Shulman GL. The reorienting system of the human brain: from environment to theory of mind. Neuron. 2008; 58:306–324. [PubMed: 18466742]

Corbetta M, Shulman GL. Control of goal-directed and stimulus-driven attention in the brain. Nat Rev Neurosci. 2002; 3:201–215. [PubMed: 11994752]

DeLong, MR., Georgopoulos, AP. Motor functions of the basal ganglia. In: Bookhard, JM.Mountcastle, VB., Brooks, VB., editors. Handbook of Physiology, Section 1, The Nervous System. American Physiology Society; Bethesda: 1981. p. 1017-1061.

Di Martino A, Scheres A, Margulies DS, Kelly AM, Uddin LQ, Shehzad Z, Biswal B, Walters JR, Castellanos FX, Milham MP. Functional connectivity of human striatum: a resting state fMRI study. Cereb Cortex. 2008; 18:2735–2747. [PubMed: 18400794]

Draganski B, Kherif F, Kloppel S, Cook PA, Alexander DC, Parker GJ, Deichmann R, Ashburner J, Frackowiak RS. Evidence for segregated and integrative connectivity patterns in the human Basal Ganglia. J Neurosci. 2008; 28:7143–7152. [PubMed: 18614684]

Everitt BJ, Belin D, Economidou D, Pelloux Y, Dalley JW, Robbins TW. Review. Neural mechanisms underlying the vulnerability to develop compulsive drug-seeking habits and addiction. Philos Trans R Soc Lond B Biol Sci. 2008; 363:3125–3135. [PubMed: 18640910]

Everitt BJ, Robbins TW. Neural systems of reinforcement for drug addiction: from actions to habits to compulsion. Nat Neurosci. 2005; 8:1481–1489. [PubMed: 16251991]

Fadardi JS, Cox WM. Reversing the sequence: reducing alcohol consumption by overcoming alcohol attentional bias. Drug Alcohol Depend. 2009; 101:137–145. [PubMed: 19193499]

Field M, Cox WM. Attentional bias in addictive behaviors: a review of its development, causes, and consequences. Drug Alcohol Depend. 2008; 97:1–20. [PubMed: 18479844]

Franken IH. Drug craving and addiction: integrating psychological and neuropsychopharmacological approaches. Prog Neuropsychopharmacol Biol Psychiatry. 2003; 27:563–579. [PubMed: 12787841]

Fuster, J. The Prefrontal Cortex. fourth. Academic Press; Boston: 2008.

Garavan H, Pankiewicz J, Bloom A, Cho JK, Sperry L, Ross TJ, Salmeron BJ, Risinger R, Kelley D, Stein EA. Cue-induced cocaine craving: neuroanatomical specificity for drug users and drug stimuli. Am J Psychiatry. 2000; 157:1789–1798. [PubMed: 11058476]

Geissler A, Lanzenberger R, Barth M, Tahamtan AR, Milakara D, Gartus A, Beisteiner R. Influence of fMRI smoothing procedures on replicability of fine scale motor localization. Neuroimage. 2005; 24:323–331. [PubMed: 15627575]

Gerbella M, Borra E, Mangiaracina C, Rozzi S, Luppino G. Corticostriate projections from areas of the "Lateral Grasping Network": evidence for multiple hand-related input channels. Cereb Cortex. 2015; 26:3096–3115. [PubMed: 26088968]

Grant S, London ED, Newlin DB, Villemagne VL, Liu X, Contoreggi C, Phillips RL, Kimes AS, Margolin A. Activation of memory circuits during cue-elicited cocaine craving. Proc Natl Acad Sci USA. 1996; 93:12040–12045. [PubMed: 8876259]

Graybiel AM, Rauch SL. Toward a neurobiology of obsessive-compulsive disorder. Neuron. 2000; 28:343–347. [PubMed: 11144344]

Haber SN, Kim KS, Mailly P, Calzavara R. Reward-related cortical inputs define a large striatal region in primates that interface with associative cortical connections, providing a substrate for incentive-based learning. J Neurosci. 2006; 26:8368–8376. [PubMed: 16899732]

Haber SN, Lynd-Balta E, Mitchell SJ. The organization of the descending ventral pallidal projections in the monkey. J Comp Neurol. 1993; 329:111–128. [PubMed: 8454722]

Haber, SN., Adler, A., Bergman, H. The basal ganglia. In: Mai, JK., Paxinos, G., editors. The Human Nervous System. Academic Press; San Diego: 2012. p. 680-740.

Hayes JP, Vanelzakker MB, Shin LM. Emotion and cognition interactions in PTSD: a review of neurocognitive and neuroimaging studies. Front Integr Neurosci. 2012; 6:89. [PubMed: 23087624]

Heilbronner SR, Haber SN. Frontal cortical and subcortical projections provide a basis for segmenting the cingulum bundle: implications for neuroimaging and psychiatric disorders. J Neurosci. 2014; 34:10041–10054. [PubMed: 25057206]

Heimer, L., Wilson, RD. The subcortical projections of the allocortex: similarities in the neural associations of the hippocampus, the piriform cortex, and the neocortex. In: Santini, M., editor. Golgi Centennial Symposium: Perspectives in Neurobiology. Raven Press; New York: 1975. p. 177-193.

Hickey C, Chelazzi L, Theeuwes J. Reward changes salience in human vision via the anterior cingulate. J Neurosci. 2010; 30:11096–11103. [PubMed: 20720117]

Holmes AJ, Hollinshead MO, O'Keefe TM, Petrov VI, Fariello GR, Wald LL, Fischl B, Rosen BR, Mair RW, Roffman JL, Smoller JW, Buckner RL. Brain Genomics Superstruct Project initial data release with structural, functional, and behavioral measures. Sci Data. 2015; 2:150031. [PubMed: 26175908]

Institute of Laboratory Animal Resources, C.o L.S., National Research Council. Guide for the Care and Use of Laboratory Animals. National Academy Press; Washington, D.C.: 1996.

Jarbo K, Verstynen TD. Converging structural and functional connectivity of orbitofrontal, dorsolateral prefrontal, and posterior parietal cortex in the human striatum. J Neurosci. 2015; 35:3865–3878. [PubMed: 25740516]

Jenkinson M, Beckmann CF, Behrens TE, Woolrich MW, Smith SM. FSL. Neuroimage. 2012; 62:782–790. [PubMed: 21979382]

Jo HJ, Lee JM, Kim JH, Choi CH, Gu BM, Kang DH, Ku J, Kwon JS, Kim SI. Artificial shifting of fMRI activation localized by volume- and surface-based analyses. Neuroimage. 2008; 40:1077–1089. [PubMed: 18291680]

Jo HJ, Lee JM, Kim JH, Shin YW, Kim IY, Kwon JS, Kim SI. Spatial accuracy of fMRI activation influenced by volume- and surface-based spatial smoothing techniques. Neuroimage. 2007; 34:550–564. [PubMed: 17110131]

Kelly RM, Strick PL. Macro-architecture of basal ganglia loops with the cerebral cortex: use of rabies virus to reveal multisynaptic circuits. Prog Brain Res. 2004; 143:449–459. [PubMed: 14653187]

Kilts CD, Kennedy A, Elton A, Tripathi SP, Young J, Cisler JM, James GA. Individual differences in attentional bias associated with cocaine dependence are related to varying engagement of neural processing networks. Neuropsychopharmacology. 2014; 39:1135–1147. [PubMed: 24196947]

Koster E, Crombez G, Van Damme S, Verschuere B, De Houwer J. Signals for threat modulate attentional capture and holding: fear-conditioning and extinction during the exogenous cueing task. Cogn Emot. 2005; 19:771–780.

Kremer JR, Mastronarde DN, McIntosh JR. Computer visualization of three-dimensional image data using IMOD. J Struct Biol. 1996; 116:71–76. [PubMed: 8742726]

Kuckertz JM, Amir N, Boffa JW, Warren CK, Rindt SE, Norman S, Ram V, Ziajko L, Webb-Murphy J, McLay R. The effectiveness of an attention bias modification program as an adjunctive treatment for post-traumatic stress disorder. Behav Res Ther. 2014; 63:25–35. [PubMed: 25277496]

Kühn S, Gallinat J. Common biology of craving across legal and illegal drugs - a quantitative meta-analysis of cue-reactivity brain response. Eur J Neurosci. 2011; 33:1318–1326. [PubMed: 21261758]

Künzle H. An autoradiographic analysis of the efferent connections from premotor and adjacent prefrontal regions (areas 6 and 9) in macaca fascicularis. Brain Behav Evol. 1978; 15:185–234. [PubMed: 99205]

Leh SE, Ptito A, Chakravarty MM, Strafella AP. Fronto-striatal connections in the human brain: a probabilistic diffusion tractography study. Neurosci Lett. 2007; 419:113–118. [PubMed: 17485168]

Lehéricy S, Ducros M, Van de Moortele PF, Francois C, Thivard L, Poupon C, Swindale N, Ugurbil K, Kim DS. Diffusion tensor fiber tracking shows distinct corticostriatal circuits in humans. Ann Neurol. 2004; 55:522–529. [PubMed: 15048891]

Levy BJ, Wagner AD. Cognitive control and right ventrolateral prefrontal cortex: reflexive reorienting, motor inhibition, and action updating. Ann NY Acad Sci. 2011; 1224:40–62. [PubMed: 21486295]

Maas LC, Lukas SE, Kaufman MJ, Weiss RD, Daniels SL, Rogers VW, Kukes TJ, Renshaw PF. Functional magnetic resonance imaging of human brain activation during cue-induced cocaine craving. Am J Psychiatry. 1998; 155:124–126. [PubMed: 9433350]

Mazza M, Tempesta D, Pino MC, Catalucci A, Gallucci M, Ferrara M. Regional cerebral changes and functional connectivity during the observation of negative emotional stimuli in subjects with post-traumatic stress disorder. Eur Arch Psychiatry Clin Neurosci. 2013; 263:575–583. [PubMed: 23385487]

Mueller-Pfeiffer C, Schick M, Schulte-Vels T, O'Gorman R, Michels L, Martin-Soelch C, Blair JR, Rufer M, Schnyder U, Zeffiro T, Hasler G. Atypical visual processing in posttraumatic stress disorder. Neuroimage Clin. 2013; 3:531–538. [PubMed: 24371791]

Pandya DN, Seltzer B. Intrinsic connections and architectonics of posterior parietal cortex in the rhesus monkey. J Comp Neurol. 1982; 204:196–210. [PubMed: 6276450]

Paxinos, G., Huang, XF., Toga, AW. The Rhesus Monkey in Stereotaxic Coordinates. Academic Press; San Diego: 2000.

Preuss TM, Goldman-Rakic PS. Myelo-and cytoarchitecture of the granular frontal cortex and surrounding regions in the strepsirhine primate galago and the anthropoid primate macaca. J Comp Neurol. 1991; 310:429–474. [PubMed: 1939732]

Robinson TE, Berridge KC. The neural basis of drug craving: an incentive-sensitization theory of addiction. Brain Res Rev. 1993; 18:247–291. [PubMed: 8401595]

Robinson TE, Berridge KC. Incentive-sensitization and addiction. Addiction. 2001; 96:103–114. [PubMed: 11177523]

Rolls, ET. The functions of the orbitofrontal cortex. In: Stuss, DT., Knight, RT., editors. Principles of Frontal Lobe Function. Oxford University Press, Inc.; New York: 2002. p. 354-375.

Rushworth MF, Hadland KA, Paus T, Sipila PK. Role of the human medial frontal cortex in task switching: a combined fMRI and TMS study. J Neurophysiol. 2002; 87:2577–2592. [PubMed: 11976394]

Sacchet MD, Knutson B. Spatial smoothing systematically biases the localization of reward-related brain activity. Neuroimage. 2013; 66:270–277. [PubMed: 23110886]

Schmidt LJ, Belopolsky AV, Theeuwes J. Attentional capture by signals of threat. Cogn Emot. 2015; 29:687–694. [PubMed: 24899117]

Schoorl M, Putman P, Van Der Does W. Attentional bias modification in posttraumatic stress disorder: a randomized controlled trial. Psychother Psychosom. 2013; 82:99–105. [PubMed: 23295710]

Selemon LD, Goldman-Rakic PS. Longitudinal topography and interdigitation of corticostriatal projections in the rhesus monkey. J Neurosci. 1985; 5:776–794. [PubMed: 2983048]

Smith SM, Jenkinson M, Woolrich MW, Beckmann CF, Behrens TE, Johansen-Berg H, Bannister PR, De Luca M, Drobnjak I, Flitney DE, Niazy RK, Saunders J, Vickers J, Zhang Y, De Stefano N, Brady JM, Matthews PM. Advances in functional and structural MR image analysis and implementation as FSL. Neuroimage. 2004; 23(Suppl. 1):S208–S219. [PubMed: 15501092]

Steinmetz MA, Constantinidis C. Neurophysiological evidence for a role of posterior parietal cortex in redirecting visual attention. Cereb Cortex. 1995; 5:448–456. [PubMed: 8547791]

Toni I, Schluter ND, Josephs O, Friston K, Passingham RE. Signal-, set-and movement-related activity in the human brain: an event-related fMRI study. Cereb Cortex. 1999; 9:35–49. [PubMed: 10022494]

Venkatraman V, Huettel SA. Strategic control in decision-making under uncertainty. Eur J Neurosci. 2012; 35:1075–1082. [PubMed: 22487037]

Verstynen TD, Badre D, Jarbo K, Schneider W. Microstructural organizational patterns in the human corticostriatal system. J Neurophysiol. 2012; 107:2984–2995. [PubMed: 22378170]

Vogt, BA. Structural organization of cingulate cortex: areas, neurons and somatodendritic receptors. In: Vogt, BA., Gabriel, M., editors. Neurobiology of Cingulate Cortex and Limbic Thalamus. Birkhäuser; Boston: 1993. p. 19-170.

Vogt, BA. Architecture, neurocytology and comparative organization of monkey and human cingulate cortices. In: Vogt, BA., editor. Cingulate Neurobiology and Disease. Oxford University Press; Oxford: 2009. p. 66-93.

White T, O'Leary D, Magnotta V, Arndt S, Flaum M, Andreasen NC. Anatomic and functional variability: the effects of filter size in group fMRI data analysis. Neuroimage. 2001; 13:577–588. [PubMed: 11305887]

Woodward TS, Ruff CC, Ngan ETC. Short- and long-term changes in anterior cingulate activation during resolution of task-set competition. Brain Res. 2006; 1068:161–169. [PubMed: 16376861]

Yeo BT, Krienen FM, Sepulcre J, Sabuncu MR, Lashkari D, Hollinshead M, Roffman JL, Smoller JW, Zollei L, Polimeni JR, Fischl B, Liu H, Buckner RL. The organization of the human cerebral cortex estimated by intrinsic functional connectivity. J Neurophysiol. 2011; 106:1125–1165. [PubMed: 21653723]

Yeterian EH, Pandya DN. Striatal connections of the parietal association corticies in rhesus monkeys. J Comp Neurol. 1993; 332:175–197. [PubMed: 8331211]

Yeterian EH, Van Hoesen GW. Cortico-striate projections in the rhesus monkey: the organization of certain cortico-caudate connections. Brain Res. 1978; 139:43–63. [PubMed: 413609]

Yin HH, Knowlton BJ. The role of the basal ganglia in habit formation. Nat Rev Neurosci. 2006; 7:464–476. [PubMed: 16715055]

Ziaee SS, Fadardi JS, Cox WM, Yazdi SA. Effects of attention control training on drug abusers' attentional bias and treatment outcome. J Consult Clin Psychol. 2016 Epub ahead of print.

Fig. 1.

Prefrontal projections to the striatum. Coronal slices are shown of projections from 6 functionally diverse prefrontal regions to the striatum. Dense projection fields are outlined and shaded black. Surrounding diffuse projection fibers are not shown. Injection sites are shaded black in smaller adjacent coronal sections of the cortex. Note that all of these functionally diverse prefrontal projections terminate in the rdCaud, indicated by red arrows. Cd=caudate. Pu=putamen. dlPFC=dorsolateral prefrontal cortex. vlPFC=ventrolateral PFC. dmPFC=dorsomedial PFC. dACC=dorsal anterior cingulate cortex. OFC=orbitofrontal cortex. (For interpretation of the references to color in this figure legend, the reader is referred to the web version of this article.)

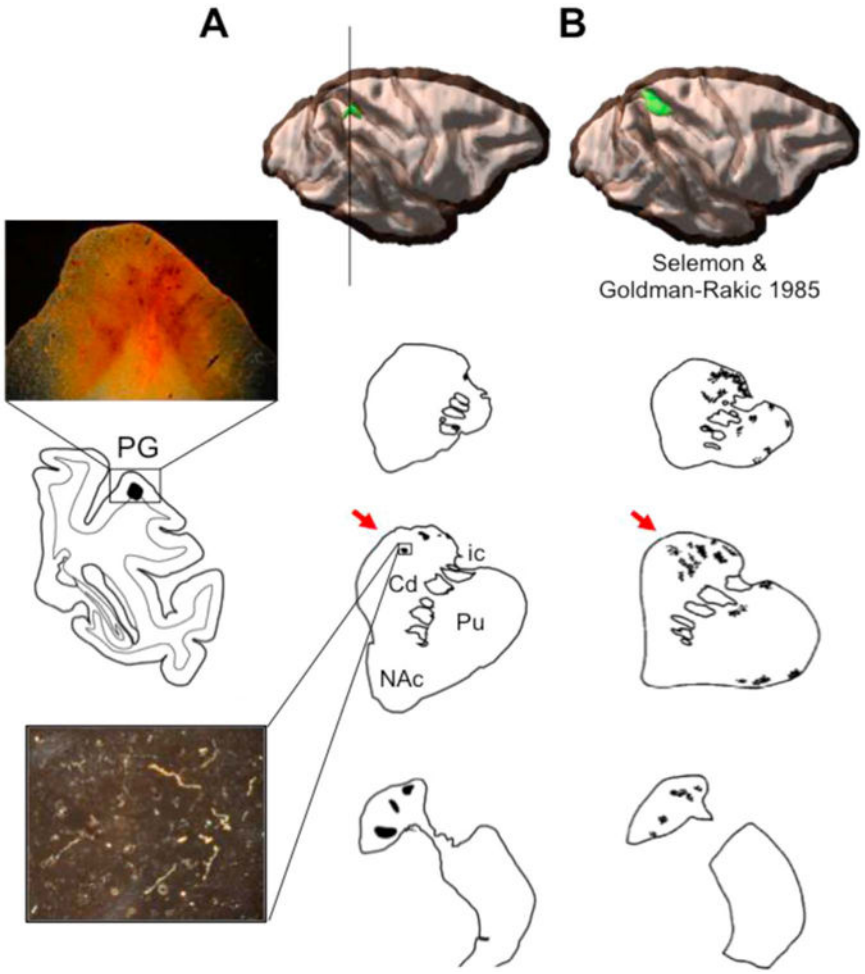

Fig. 2.

Caudal IPL projections to the striatum. (A) An anterograde tracer injection (green) was placed in area PG of the caudal IPL. Coronal sections show dense projection patches (shaded black) through the striatum. Black line through cortex indicates a coronal slice of the injection site shown to the left with an inset 2× microphotograph. Below, a 10× microphotograph of a dense fiber patch in the rdCaud. (B) Coronal striatal sections from a larger, tritiated amino acid tracer injection (modeled in 3-D) in the caudal IPL reported in the literature. Note that in both cases caudal IPL projections terminate in the rdCaud, indicated by red arrows. Cd=caudate. Pu=putamen. NAc=nucleus accumbens. ic=internal capsule. Images adapted and republished with permission of Society for Neuroscience, from Selemon and Goldman-Rakic (1985); permission conveyed through Copyright Clearance Center, Inc. (For interpretation of the references to color in this figure legend, the reader is referred to the web version of this article.)

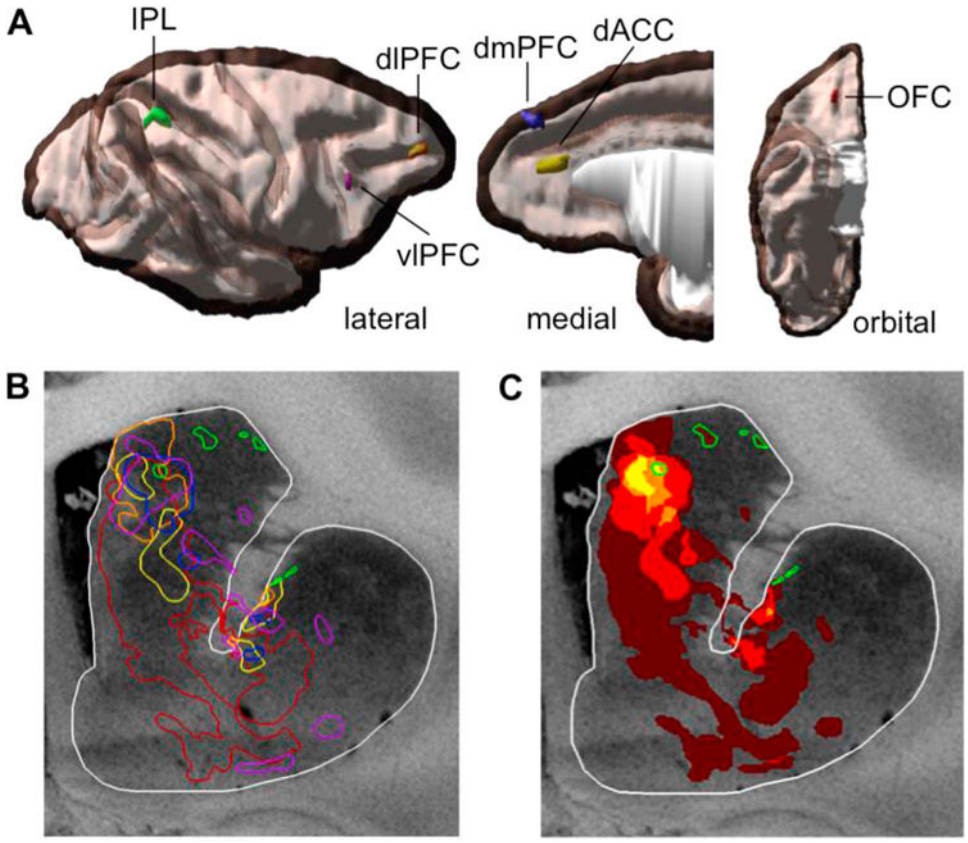

Fig. 3.

Overlay of prefrontal and parietal dense projections in the striatum. (A) 3-D rendering of cortical injection sites in the prefrontal and parietal cortices. Injections shown on opaque white matter and translucent gray matter. (B) A coronal section of the striatum at an area of greatest convergence of dense projections. Dense projection patches are outlined in the same colors as their cortical injections. (C) Heatmap showing overlap of dense projections in the same coronal section. IPL projections are highlighted in green. Note the area of convergence in the medial rdCaud with the caudal IPL projections. (For interpretation of the references to color in this figure legend, the reader is referred to the web version of this article.)

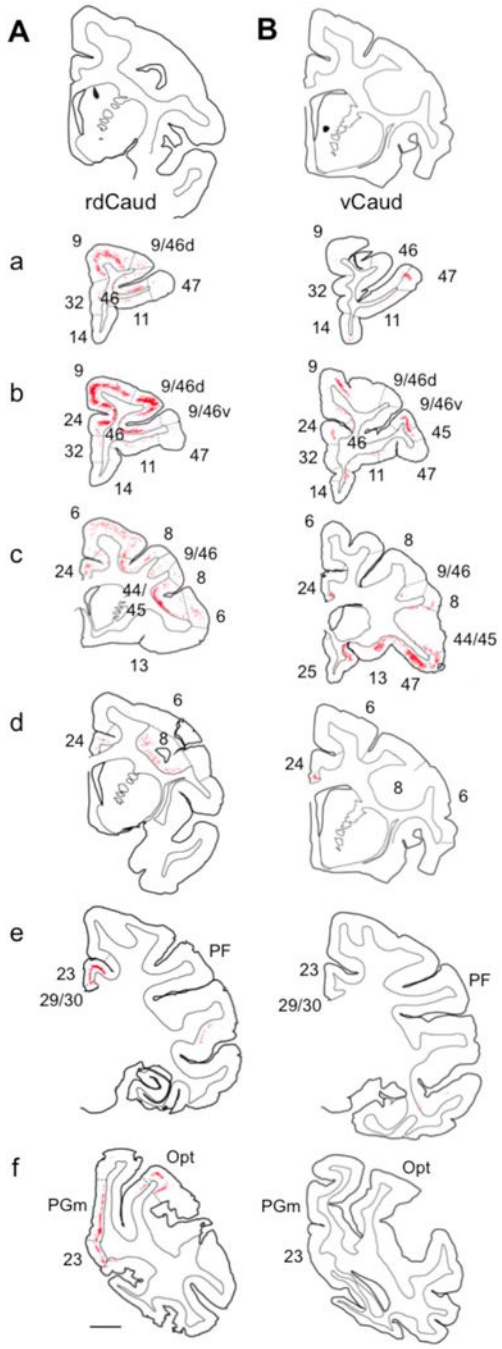

Fig. 4.

Cortical inputs to the rdCaud and vCaud. Labeled input neurons (red dots) following retrograde tracer injections in the (A) rdCaud or (B) vCaud. Injection sites (black) shown at top. (a–f) Rostral to caudal coronal sections through the brain. Numbers refer to cortical areas; dashed lines indicate approximate areal boundaries. Scale bar, 5 mm.

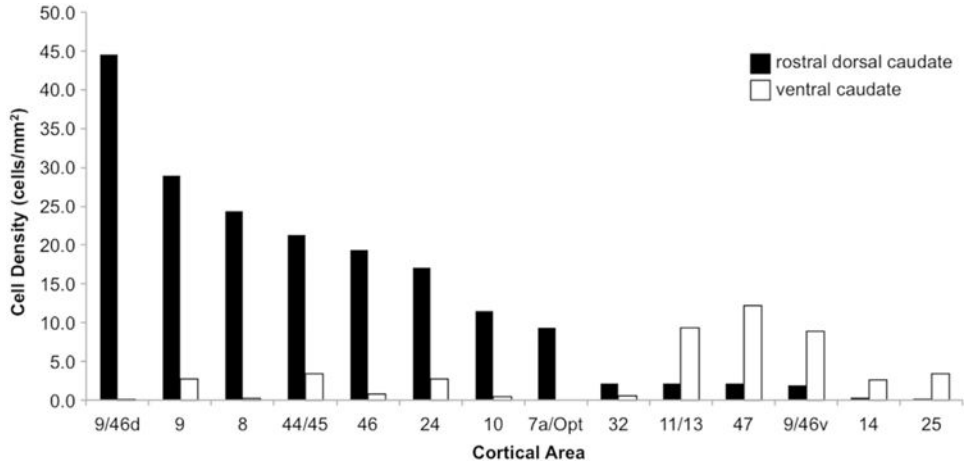

Fig. 5.

Quantification of cortical inputs to the rdCaud and vCaud. Densities of cortical input neurons by area revealed by retrograde tracer injections in the rdCaud (black bars) and vCaud (white bars). $X^2(12,100)=1560$, $p < 0.0001$.

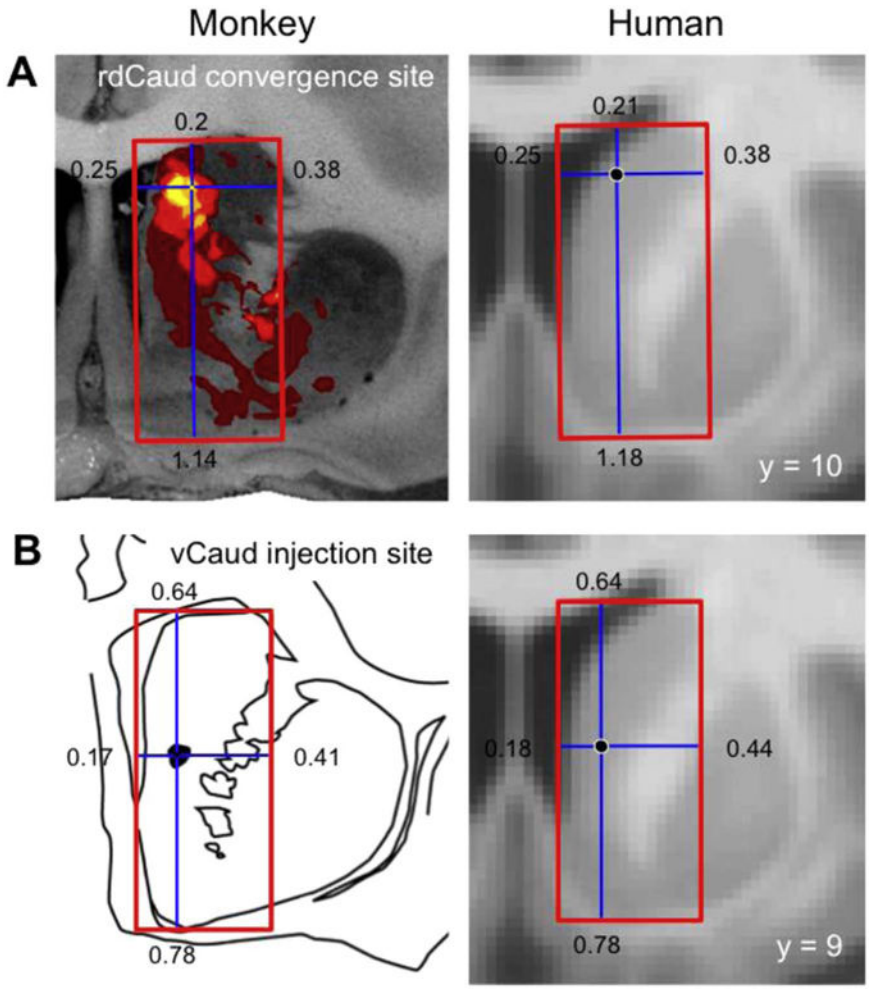

Fig. 6.

Human striatal seed region selection. Human striatal seed regions were placed in the spatially proportionate locations to (A) the greatest convergence of prefrontal and caudal IPL projections in the monkey medial rdCaud or (B) the monkey vCaud injection site. Red boxes parallel to the midline are drawn around the caudate and adjacent nucleus accumbens. Cross hairs indicate the regions of interest in the monkey and the spatially proportionate locations in the human striatum. Numbers refer to lengths of cross hair arms in an arbitrary unit.

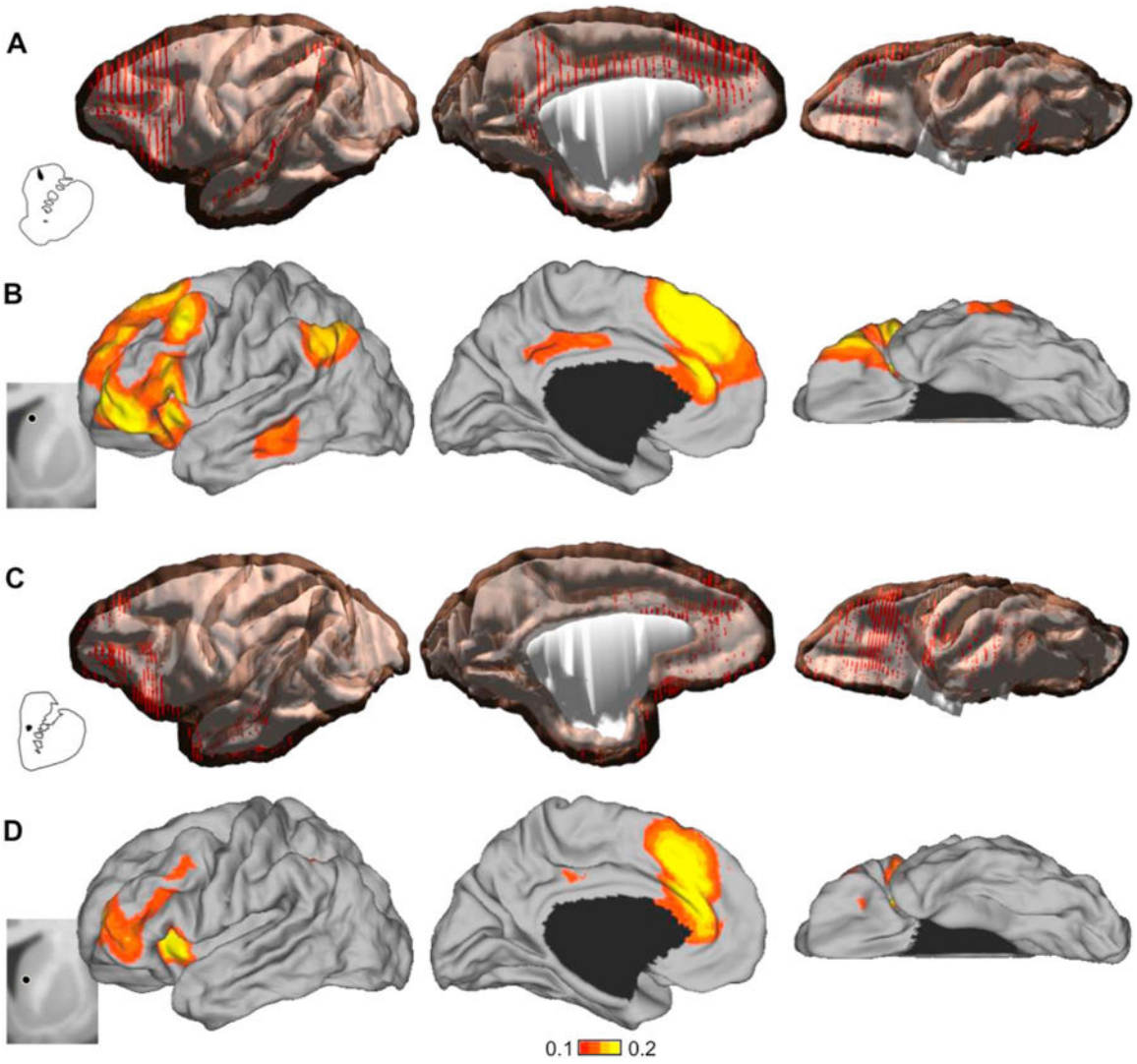

Fig. 7.

Monkey and human corticostriatal connectivity with the rdCaud and vCaud. Whole brain 3-D renderings of the retrogradely labeled cells (red dots) from the (A) rdCaud or (C) vCaud injections in monkeys. Human fcMRI maps correlating with (B) a human medial rdCaud region (−10, 10, 14) corresponding to the site of greatest convergence in the monkey medial rdCaud or (D) a human vCaud region (−9, 9, 5) corresponding to the monkey vCaud injection site. fcMRI maps were created with single 2 mm^3 voxel seed regions using data from 500 human subjects. Negative correlations are shown in Supplementary Fig. 1. Monkey injection sites and human seed regions are shown to the left. Black circles are centered on coordinates of voxel seed regions. Subcortical structures are masked medially.

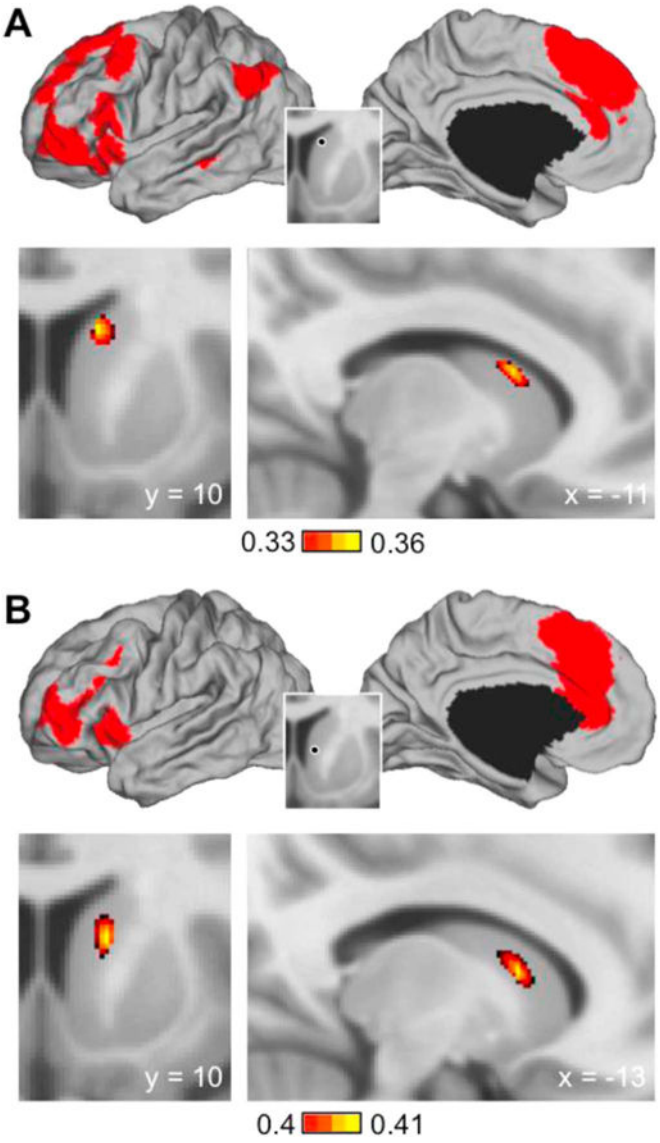

Fig. 8.

Cortical resting-state correlations in the human striatum. Striatal fcMRI maps were generated in 500 healthy human subjects with a single seed region composed of all cortical regions correlated at 1.5 standard deviations above the mean with the (A) rdCaud or (B) vCaud seed regions (see Fig. 7). Cortical seed regions are shown above in red; inset shows original striatal seed regions used to identify cortical seed regions. Coronal and sagittal sections below show the site of the peak correlation in the striatum. Peak correlations were located at −11, 10, 15 and −13, 10, 10 for rdCaud and vCaud, respectively. Negative correlations in Supplementary Fig. 2. Note that for the medial rdCaud, the peak correlation is also located in the medial rdCaud, while for the vCaud, the peak correlation is located elsewhere in the striatum.